Supplement of Atmos. Chem. Phys., 22, 5651–5663, 2022
https://doi.org/10.5194/acp-22-5651-2022-supplement

Atmospheric Chemistry and Physics
Open Access
EGU

Supplement of

Aqueous chemical bleaching of 4-nitrophenol brown carbon by hydroxyl radicals; products, mechanism, and light absorption

Bartłomiej Witkowski et al.

Correspondence to: Bartłomiej Witkowski (bwitk@chem.uw.edu.pl)

S1. Materials and reagents

All reagents were at least ACS reagent grade or higher and were used without any further purification. 4-nitrophenol (≥99%), hydroquinone (≥99.5%), 4-nitrocatechol (≥97%), 1,2,4-trihydroxybenzene (≥99%), 2-nitrophloroglucinol (95%), phloroglucinol (≥99.5%), hydrogen peroxide (H_2O_2) solution in water (≥30% ultra-trace with no stabilizers added), acetic anhydride (≥99%), sodium chloride (≥99%), sodium phosphate dibasic (≥99%), HPLC-grade solvents: ethyl acetate (≥99.5%), methanol (≥99.9%) as well as the plastic, single-use cuvettes (P/N Z637157) with 1 cm optical pathway length and the effective wavelength range 230-900 nm were all purchased from Sigma Aldrich (Schnelldorf, Germany). Anhydrous sodium sulfate (fine powder, ≥99%), sodium hydroxide (≥99%), hydrochloric acid (35-37% solution in water) were obtained from Avantor Performance Materials (Gliwice, Poland). Perchloric acid (65% solution in water) was obtained from Chempur (Piekary Śląskie, Poland). Deionized (DI) water (18 MΩ × cm^{-1}) was prepared with the Direct - Q3 Ultrapure Water System (Millipore). Ultra-high purity (UHP) helium (carrier gas for GC/MS) and UHP oxygen (used in the total organic carbon analyzer) were supplied by Multax (Stare Babice, Poland).

S2. Acid-base equilibrium of 4-nitrophenol in water

The pK_a value of 4-nitrophenol (4NP) was previously reported as ca. 7.15 (Vione et al., 2009; Zhao et al., 2015) and it was used to evaluate the concentration ratio of protonated and deprotonated forms of this compound under the experimental conditions used.

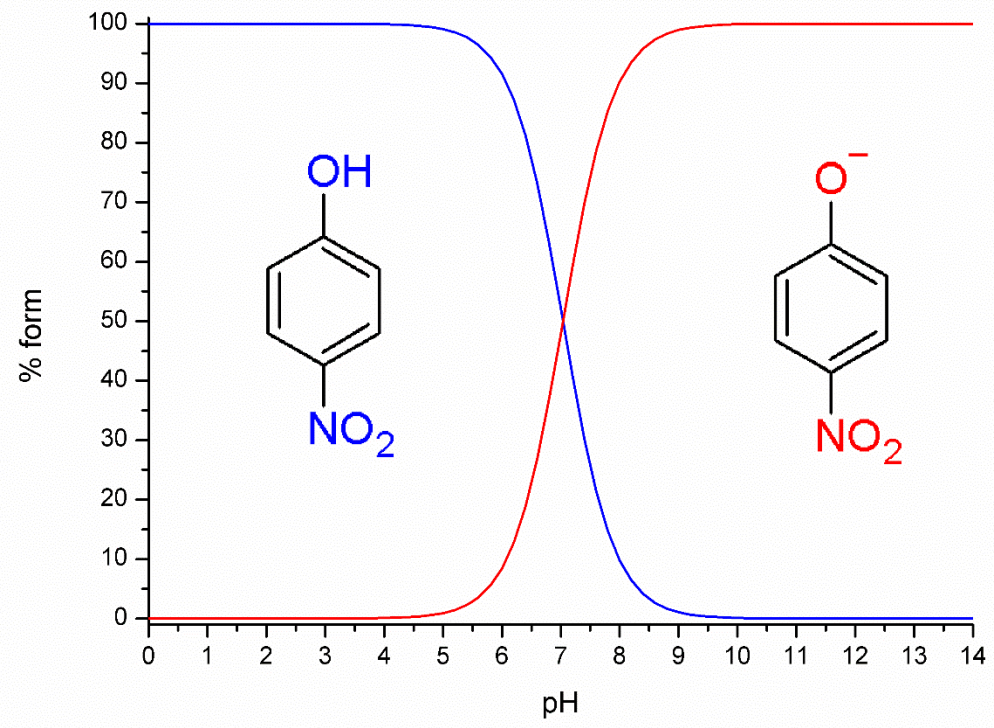

Figure S1: Dissociation curve of 4NP as a function of pH.

As presented in Fig. S1, at pH=2 or pH=9, 4NP was present in the aqueous solution as completely protonated or as nitrophenolate ion, respectively. Hence, under the experimental conditions used in this work, it was possible to investigate the OH reaction with completely protonated and deprotonated forms of 4NP

S3. The steady state concentration of hydroxyl radicals in the absence of organic reactants.

The concentration of OH in the absence of organic reactants was estimated by monitoring the disappearance of H_2O_2 in DI water following photolysis in the photoreactor at 298 K (section S2.1). The first-order rate constant of photolysis was then estimated with a kinetic box model (Tan et al., 2009) – results are presented in Fig. S2.

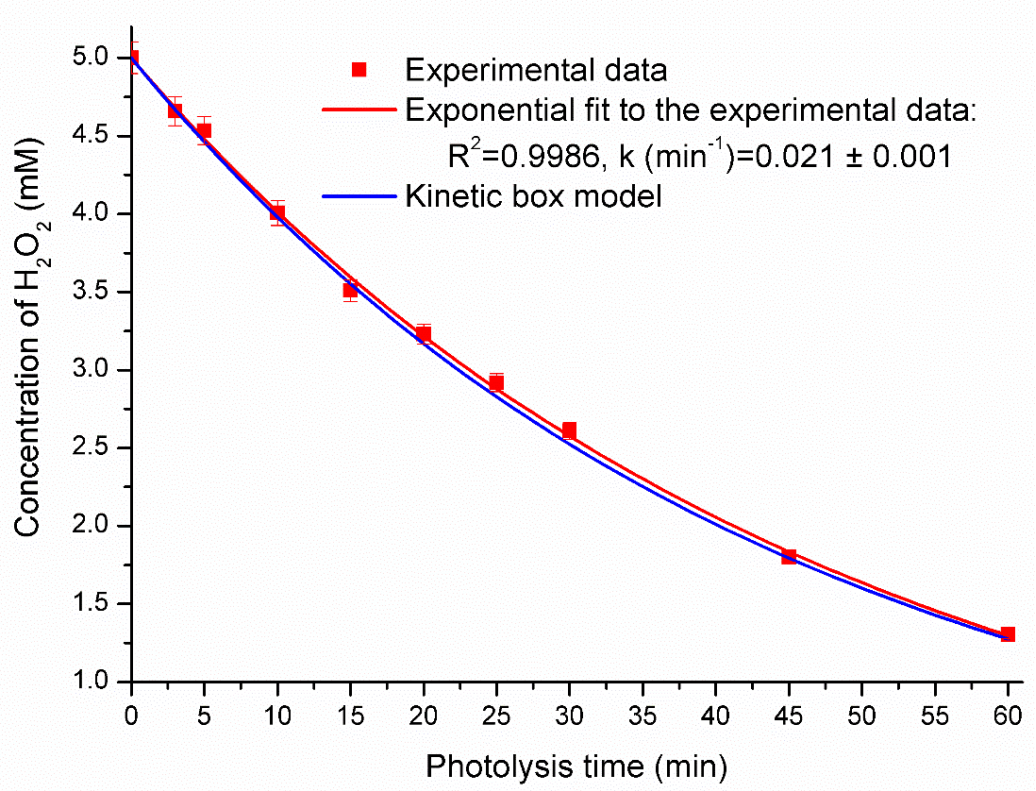

Figure S2: Photolysis of H2O2 in the photochemical reactor.

As presented in Fig. S2, the kinetic box model accurately reproduced the photolysis of H_2O_2 and a first-order photolysis rate constant of 1.9×10^{-4} s^{-1} was obtained. The estimated steady-state concentration of OH in the absence of organic reactants was 1.4×10^{-9} M. This value is much higher than the upper limit of OH concentration in cloud water but here it is used for simulating the aqueous chemical processing of 4NP via OH within a reasonable time-scale.

S4. Experimental details

S4.1. Photooxidation of 4-nitrophenol in the aqueous photoreactor

The photooxidation reaction was carried out in a custom-made quartz, jacketed reaction vessel with the internal volume of 100 ml. The reaction vessel was closed with a glass stopper and placed inside the photochemical reactor which is described in more detail elsewhere (Witkowski et al., 2019).

The reaction mixture consisted of deionized water and 4NP (concentration between 100 and 350 μM) and the pH was unbuffered (no acids or buffers added) or it was adjusted to 2 or 9 with HCl, $HClO_4$, or Na_2HPO_4. The pH was checked with the HI 221 pH-meter (Hanna Instruments) before and after each experiment. The pH meter was calibrated daily with pH=4.01, 7.00, and 10.00 buffer solutions. After adjusting the pH, the reaction solution was filtered through a 1.2 μm glass microfiber syringe filter and transferred into the reaction vessel. The zero-time sample was withdrawn from the reactor and then H_2O_2 was added (the initial concentration of H_2O_2 in the reaction mixture was ca. 5 mM - Fig. S2). Aliquots of the reaction mixture were withdrawn periodically from the photoreactor at five minutes intervals and the total reaction time was 60 min.

Photoreactor used in this work was equipped with a circular set of eight 4W, G5-socket lamps. Out of all eight lamps in the photoreactor, two were UVC, mercury lamps with the peak emission at 254 nm (TUV TL 4W, Philips). The UVC lamps were placed opposite to each other for a symmetric irradiation of the reaction mixture. The other six lamps were emitting visible light above 400nm. Such a mixed set of lamps was used to limit the amount of short-wavelength UVC irradiation in order to avoid direct photolysis of phenols under investigation (Table S1). At the same time, the amount of UVC irradiation was sufficient to efficiently produce OH via H_2O_2 photolysis. Hence, it was possible to investigate the 4NP reaction with the OH while avoiding direct photolysis of the reactants – see also section S4.2.

The reactor lamps were allowed to warm up for at least 30 min prior starting of the experiment. The fan placed at the bottom of the photoreactor prevented the lamps from overheating by forcing the air to flow through the inside portion of the circular set of lamps. The stirring bar was placed inside the reaction vessel for the continuous stirring of the mixture with a bullied-in magnetic stirrer. The water was circulated in the outer jacket of the quartz reaction vessel to maintain the temperature of the reaction mixture at 298 K using a circulating bath (SC100 a10, Thermo Fisher Scientific).

S4.2. Quantification of phenolic products with gas chromatography coupled to mass spectrometry

The sample volume was 250µl; each sample of the reaction mixture was added to a 2.5 ml of the aqueous solution of Na_2HPO_4 (concentration 20 g/L, pH=7.4) and NaCl (concentration 28 g/L) in a 4 ml glass vial and immediately derivatized. 10 µl of phloroglucinol (internal standard) solution in DI water (concentration 0.5 g/L) was added followed by 20 µl of acetic anhydrite; the derivatization reaction was carried out for 1h. After 1h, each aqueous sample was extracted with 300 µl of ethyl acetate via mechanical agitation for ca. 20 s. The top organic layer was separated, dried with the anhydrous Na_2SO_4 via mechanical agitation and then centrifuged for 10 min in order to separate the solid residue from the organic layer. The organic layer was transferred into a separate vial with a 300 µl fused-in glass insert and 1µl of the dried ethyl acetate was injected into GC/MS. GC/MS analyses were carried out using GC-MS-QP2010 Ultra gas chromatograph (Shimadzu) interfaced with the single quadrupole QP-5000 mass spectrometer (Shimadzu). The instrument was equipped with an AOC-5000 autosampler (Shimadzu) that was used in the liquid-injection mode and equipped with a 10 µl syringe. The syringe was washed five times before and after each injection, firstly with 8µl of methanol and subsequently with 8µl ethyl acetate. The purpose of this extensive washing of the syringe was to avoid the accumulation of the solid Na_2SO_4 that caused clogging of the syringe needle and prevented the plunger from moving smoothly as inferred from the initial experiments.

The analytes were separated using capillary column ZB-5MSPlus (Phenomenex): 30m × 0.25mm, 0.25 µm of the stationary phase. The column head pressure was 26.7 kPa, the total flow of the carrier gas was 10.5 ml/min, column flow 0.68 ml/min (30 cm/sec), purge flow was 3 ml/min. The linear velocity flow control mode was used and the split ratio was 10. The temperatures of the injector, ion source, and the mass spectrometer were 280°C. The following temperature program was used: initially 50 °C held for 5 min, then linear increase at the rate of 14 °C/min to 280°C, kept for 7 min, the total analysis time was 28 min. Electron impact ionization (EI) was used to ionize the analytes eluting from the capillary column and the mass spectrometer was operating in the selected ion monitoring mode (SIM) – see Table S1 - and the solvent cut was 6 min. GCMS solution 2.53 (Shimadzu) program was used for data acquisition and processing. Standards, m/z of the ions selected for the SIM mode, and the tested linearity range of the MS detector under the experimental conditions used are listed in Table S1.

Table S1. List of standards and the parameters of the GC/MS analysis method

Name	Ions monitored in SIM mode (m/z)	Retention time (min)	Concentration range ($mg \times L^{-1}$)	Squared linear coefficient of determination (R^2)
Hydroquinone	43, 110, 152	14.8	2.5-38	0.9993
4-Nitrophenol	43, 65, 81, 93, 123, 139, 181	15.1	2.5-37	0.9977
1,2,4-Trihydroxybenzene	43, 126, 168, 210	17.3	2.5-37	0.9949
4-Nitrocatechol	43, 81, 125, 139, 155, 181, 197	17.4	2.5-37	0.9949
Phloroglucinol	43, 126, 168, 210	17.6	23	*Internal standard*
4-Nitrophloroglucinol	43, 125, 153, 171, 213, 255	18.9	2.5-38	0.9981

As listed in Table S1, phloroglucinol was used as an internal standard for quantification of the phenols listed. 4-Nitrophloroglucinol was not produced via OH+4NP reaction and was used as a surrogate standard for quantification of 4-nitropyrogallol and 5-nitropyrogallol that were both detected in the reaction mixture. The sample chromatogram of the standard mixture of phenols listed in Table S1 is shown in Fig. S3.

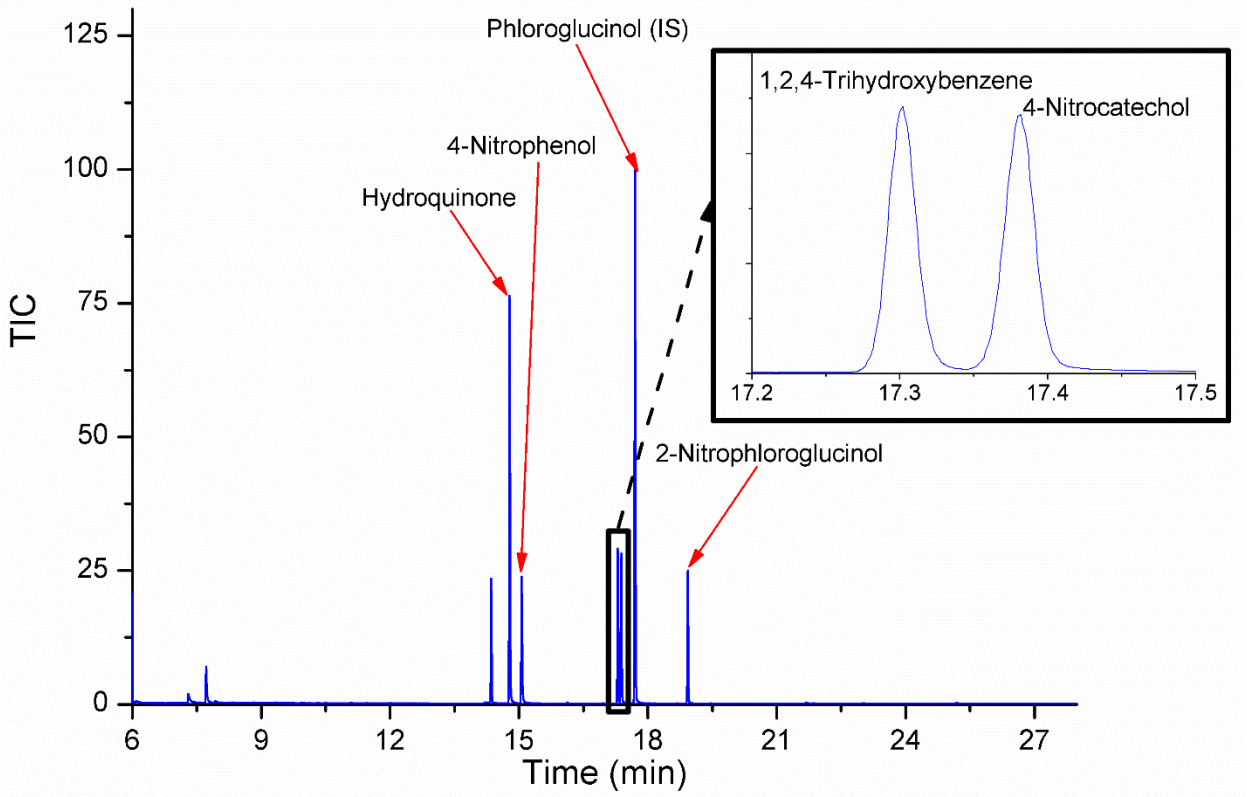

Figure S3: Chromatogram of the standard mixture of phenols listed in Table S1 detected as their acetyl derivatives.

S4.3. UV-Vis measurements

UV-Vis measurements were carried out with an i8 dual-beam spectrometer (Envisense) in 4 ml cuvettes with a 1 cm absorption pathway using plastic cuvettes with wavelength range 230-900 nm. The wavelength-dependent cross sections, ε, ($mol^{-1} \times L \times cm^{-3}$) were measured for 4NP, HH, HQL, 4-nitrocatechol, and 2-NCG at a spectral resolution of 1 nm between 230 and 600 nm. For each phenol listed, ten standard solutions were prepared with concentrations between 1 and 6×10^{-5} M. The pH of standard solutions was between 2 – 9 (changed by 1 pH unit) and was adjusted with HCl, H_3PO_4, or Na_2HPO_4.

The absorbance of the 4NP solution during the reaction with the OH (see sections 2.2 and S2.2) was measured between λ = 230 and 600 nm by periodically sampling 300 µl samples from the reaction mixture. Each 300 µl aliquot was then diluted with 2 ml of a buffer solution. After measuring the absorbance, the pH was adjusted by adding a small volume of NaOH or H_3PO_4 solution in DI water. A microelectrode was inserted directly into the UV-Vis cuvettes to measure the pH of each sample before the absorbance was recorded. After adjusting the pH, the UV-Vis spectrum was recorded again and this procedure was repeated for each sample until pH=9 was reached. The absorbance measured for each sample was corrected for the dilution using the volume of the added buffering agent.

S4.4. Total organic carbon analyses

Non-purgeable organic carbon (NPOC) was measured with a TOC-5050A analyzer (Shimadzu) equipped with the ASI-5000A autosampler (Shimadzu) to study the potential mineralization of 4NP and the formation of volatile products. Firstly, the instrument was calibrated with the standard solutions of 4NP in water with concentrations between 3 and 35 $mg_{TOC} \times L^{-1}$. Each standard solution was injected into the instrument minimum of three times. The calibration curve was obtained by plotting integrated peak area from the CO_2, resulting from mineralization of dissolved organic compounds at 650°C via platinum catalyst (depended variable), and concentration of 4NP in $mg \times L^{-1}$ (independent variable); the squared linear coefficient of determination for the calibration curve (R^2)=0.9995 was obtained.

Initially, the 1.5 ml aliquots of the reaction solution were diluted with the same volume of DI water before the analysis to adjust the initial NPOC concentration to ca. 13 $mg \times L^{-1}$. Afterward, each sample was filtered with a single-use PTFE syringe filter (pore size 0.22 µm) and the filtered solution was placed in the TOC autosampler vial. Subsequently, 50 µl of 2M HCl was added via the autosampler and each sample was purged with oxygen for 2 min before injection to remove the dissolved CO_2 and volatile organic compounds (VOCs). The injection volume was 20 µl and each sample was injected into the instrument three to five times until the value of relative standard deviation for the CO_2 peak area from three separate injections was lower than 2%.

S5. Derivation of the yields of phenolic products and kinetic box model

Table S2. Results of the linear regression analysis for the summarized yield of phenols from reaction (I) under acidic and basic pH conditions derived with eq. I – see Fig. 2 in the main text

pH=2				
Δ4NP, mM (x-axis)	**[Products], mM (y-axis)**	**Residuals from linear regression**	**Standardized residuals**	**Adjusted, squared linear coefficient of determination (R^2)**
0.00	0.000	0.000	0.000	
0.047	0.010 ± 0.001	-1.5E-05	-0.011	
0.076	0.014 ± 0.001	-0.002	-1.380	0.996
0.10	0.018 ± 0.001	-0.002	-1.529	
0.11	0.025 ± 0.002	0.001	1.067	
0.13	0.027 ± 0.002	0.001	0.743	
0.14	0.029 ± 0.002	0.000	0.260	
pH=9				
Δ4NP, mM (x-axis)	**[Products], mM (y-axis)**	**Residuals from linear regression**	**Standardized residuals**	**Adjusted, squared linear coefficient of determination (R^2)**
0.000	0.000	0.0000	0.00	
0.023	0.013 ± 0.001	0.0062	1.30	
0.038	0.018 ± 0.001	0.0062	1.30	0.978
0.060	0.022 ± 0.001	0.0036	0.77	
0.074	0.028 ± 0.001	0.0049	1.03	

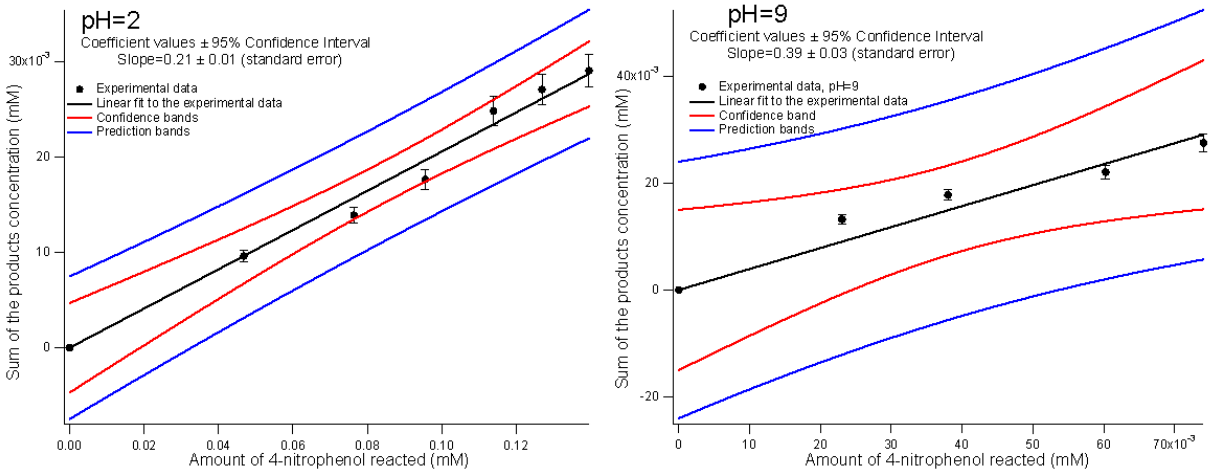

Figure S4: Results of the linear regression analysis of the data presented in Fig. 2 in the main text. Note that at a 95% confidence level, more than 95% of the points, representing the experimental data, should fall between the prediction bands. Furthermore, of the experiments are reported numerous times, 95% of the time (at the 95% confidence level), the fitted line should fall between the confidence bands.

Kinetic box model was constructed using the yields of phenolic products (primarily 4NC) derived from the experimental data and the k_{OH} values listed in the literature (Table S3).

Table S3. Reactions included in the kinetic box model

Number	Reaction	Rate constant ($M^{-1}s^{-1}$)	Comments	Reference
1	$H_2O_2 \rightarrow 2OH$	2.5×10^{-5}		
2	$OH + H_2O_2 \rightarrow HO_2 + H_2O$	2.7×10^{7}	Reactions 1-5 describe the generation of	(Tan et al.,
3	$HO_2+H_2O_2\rightarrow OH + H_2O$	3.7	the steady-state concentrating of OH via	2009)
4	$HO_2 + HO_2 \rightarrow H_2O_2 + O_2$	8.3×10^{5}	photolysis of H_2O_2	
5	$OH + HO_2 \rightarrow H_2O+O_2$	7.1×10^{5}		
6	4NP + OH → 4NC+4NP+products	4.1×10^{9}(pH=2) 8.4×10^{9}(pH=9)	The yield of 4NC and 4NP was set to 0.2 or 0.32, at pH=2 and 9, respectively	
7	4NC + OH → products	2×10^{9} (pH=2)[a]	Due to lack of the experimental data, this rate constant was fitted to the experimental data	
8	4NC + OH →4NC+ products	10×10^{9}(pH=9)[a]	This reaction was necessary to reproduce the experimental data via the box model at pH=9, yield of 4NC was set to 0.5	

[a]Best-fit value, see the discussion below

The rate constant reported for 4NC=5×10^{9} does not correspond to the fully deprotonate form of this compound first pKa≈7 (Hems and Abbatt, 2018). Also, to our knowledge, no k_{OH} values were reported for the fully protonated or partially deprotonated form of 4NC, which are dominant at pH=2 and 9, respectively. Note that 4NC has three deprotonated forms due to the presence of two hydroxyl groups but at pH=9 the deprotonation is likely to occur primarily in position 1 (first pKa≈7) (Chemaxon, 2021), yielding a singly charged 4-nitrocatecholate anion. Therefore, due to lack of the experimental data, rate constants for 4NC were optimized based on the experimental data. In other words, the rate constants for the 4NC+OH reaction were optimized to yield the best fit to the first-order decay rates. The initial concentrations were: H_2O_2 =5 mM, 4NP = 300 μM. Results of the kinetic box models, together with the experimental data are presented in Fig. S5.

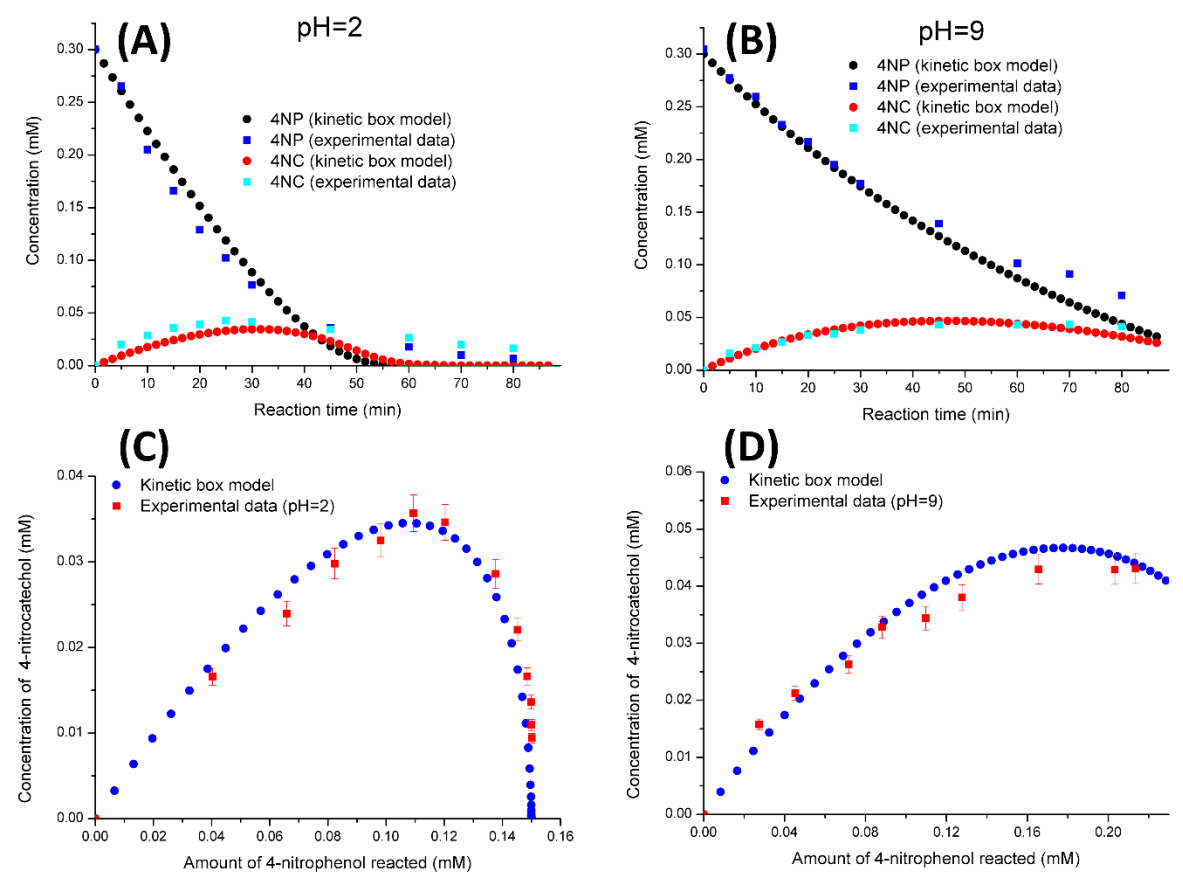

Figure S5: Results obtained with the kinetic box model together with the experimental data acquired for the reaction (I).

As presented in Fig. S5, the kinetic box model accurately reproduced the experimental data. Most importantly, the modeling results indicate the existence of an additional reaction pathway for 4-NC (deprotonated forms) under basic pH conditions, that may result in regeneration of this compound with a 0.5 yield (Table S3). Reaction 8 is likely negligible under acidic pH conditions.

At the same time, it was not possible to construct a complete kinetic model due to insufficient data available, most notably missing rate constants and branching ratios of reactions shown in Fig. 3 in the main text. Moreover, advanced kinetic modeling was beyond the scope of this work. However, the results obtained from kinetic modeling also confirmed that the non-linear trend (curving) of the plots derived with eq. (I) are due to reactions of the products (here 4NC) with the OH; reactions 7 and 8 in Table S3.

S6. UV-Vis absorption cross sections of 4NP, hydroquinone, 4-nitrocatechol, 1,2,4-trihydroxybeneze, and 2-nitrophloroglucinol

The UV-Vis absorption cross sections of 4NP, hydroquinone, 4-nitrocatechol, 1,2,4-trihydroxybeneze, and 2-nitrophloroglucinol were measured between pH 2 and 9 (section S2.3). Note that hydroquinone, 4-nitrocatechol, 1,2,4-trihydroxybeneze were unstable at pH>7, thus the ε values were not measured for these compounds at pH=8 and are not included in Fig. S6. The pH-dependent ε values measured for the five compounds between 230 and 600 nm are provided in appendix 1.

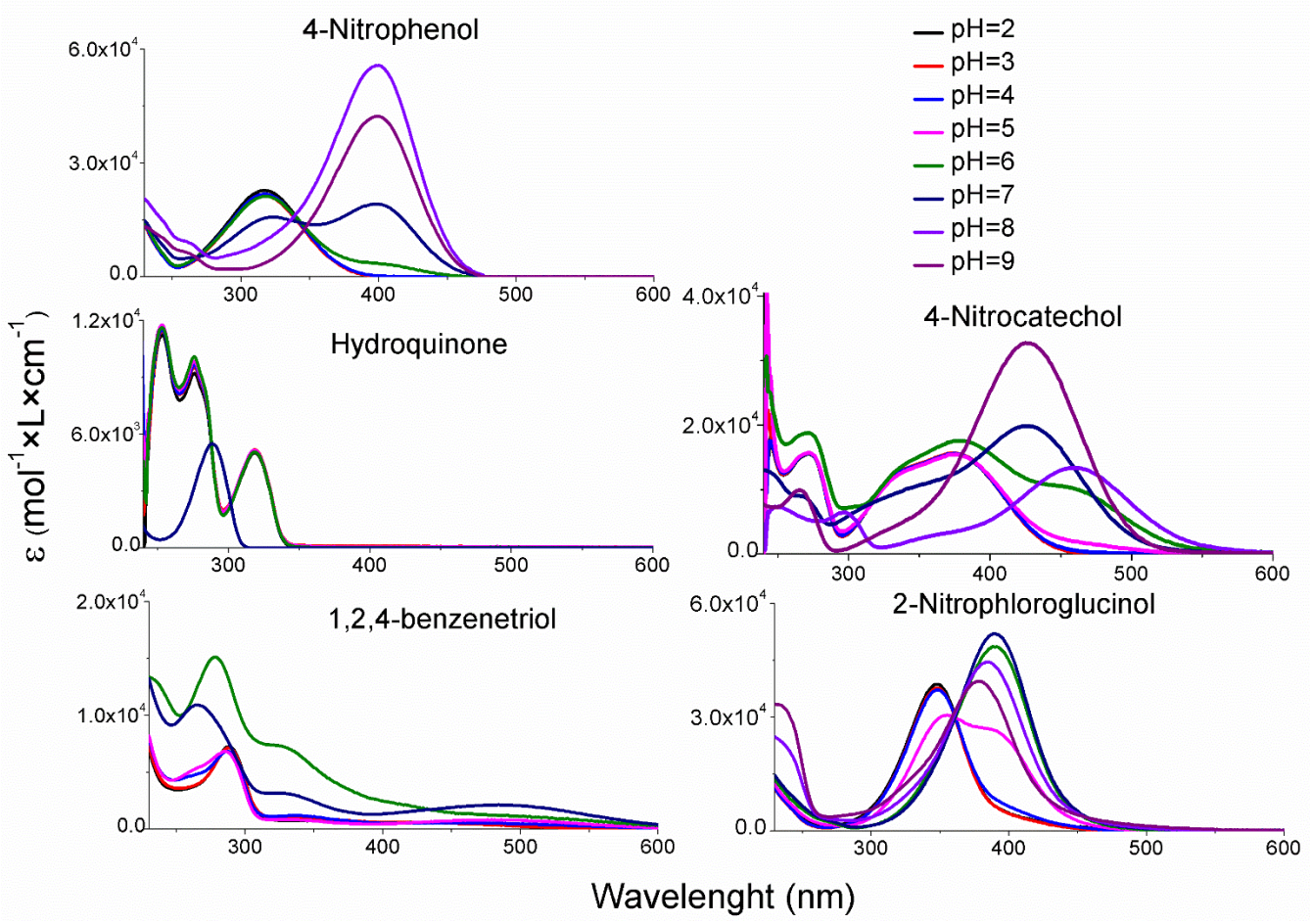

Figure S6: pH and wavelength-dependent UV-Vis absorption cross sections measured for 4NP, hydroquinone, 4-nitrocatechol, 1,2,4-trihydroxybeneze and 2-nitrophloroglucinol in water.

S7. Control experiments

Control experiments listed in Table S4 were carried out using pure 4NP or a mixture of compounds listed in Table S1. Due to a large number of control experiments, the results obtained are summarized in Table S4, for clarity. The objective of the experiments listed was to evaluate whether or not any other processes, in addition to the reaction with the OH, contributed to the formation or disappearance of phenols under the investigation.

Table S4. Experimental conditions and results of the control experiments

Compound name	Reaction conditions			Results
	pH	UV	H_2O_2	
4-Nitrophenol (precursor)	2 (HCl or $HClO_4$) or	Yes	No	
4-Nitrocatechol,	9 (Na_2HPO_4)	No	Yes	N/R
2-Nitrophloroglucinol		No UV or H_2O_2		
		Yes	No	
	2 (HCl or $HClO_4$)	No	Yes	N/R
Hydroquinone,		No UV or H_2O_2		
1,2,4-Trihydroxybenzene		Yes	No	
	7, 8, 9 (Na_2HPO_4)	No	Yes	Decomposition at pH>7
		No UV or H_2O_2		

As listed in Table S4, none of the phenols under investigation underwent direct photolysis or "dark" reactions with H_2O_2, within the time scale of the experiments. Moreover, the stability of hydroquinone and 1,2,4-trihydroxybenzene depends on the pH of the solution; these compounds either decomposed or underwent different "dark" reactions under basic pH conditions (Randolph et al., 2018). The concentration of 1,2,4-trihydroxybenzene decreased rapidly at pH>7, which is consistent with the previously published data (Liu et al., 2010).

Moreover, due to relatively fast and irreversible hydrolysis of hydroquinone and 1,2,4-trihydroxybenzene, the pH-dependent ε values for these compounds were measured at pH<7. No derivatization artifacts (e.g. phenols that were not present in the standard solutions) were detected in any of the control experiments, thereby unambiguously confirming that 4-nitroresorcinol and 4-nitropyrogallol were produced from the reaction of OH with 4NP, as it is presented in section 3.1.

2-Nitrophloroglucinol was stable in basic solution, as opposed to its structural isomers that were tentatively identified in the reaction mixture: 4-nitropyrogallol and 5-nitropyrogallol. Due to the lack of standards, the stability of these two products in basic solutions was investigated indirectly, as described in section S7.

S8. Oxidation of 4-nitrocatechol via OH under acidic and basic conditions

A separate set of experiments was carried out with 4-nitrocatechol as a precursor; the experimental conditions and GC/MS analysis procedure were the same as in the experiments with 4NP. The GC/MS chromatograms obtained are presented in Fig. S7 and S8.

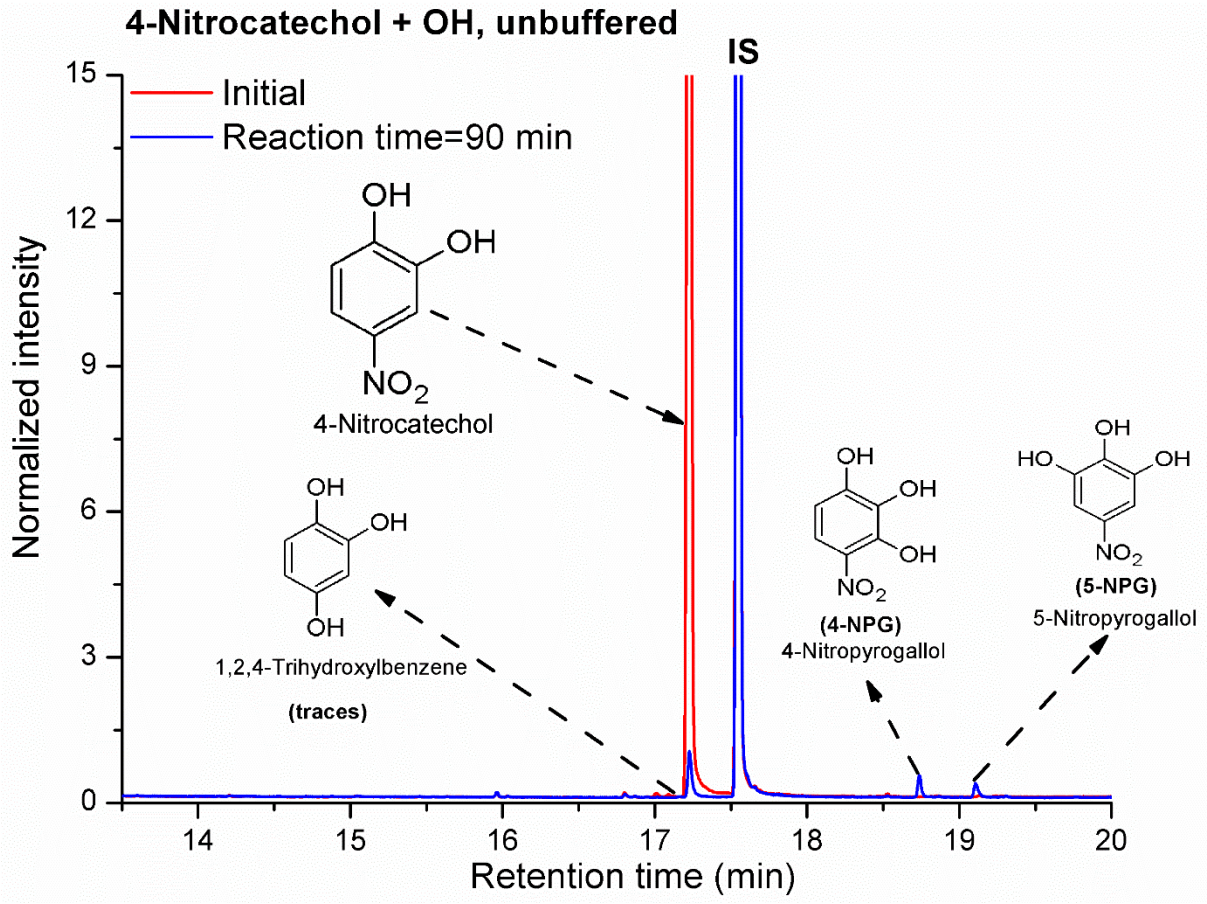

Figure S7: Chromatograms illustrating the formation of phenolic products from 4-nitrocatechol +OH reaction in pure water.

As presented in Fig. S7, the experimental data acquired unambiguously confirmed that 4-nitropyrogallol and 5-nitropyrogallol were formed following OH reaction with 4-nitrocatechol. Moreover, the formation of 1,2,4-trihydroxybenzene was not observed; only a trace amount of this product was detected in the reaction mixture. Analogously to the reaction of OH+4NC, the pH of the reaction solution quickly decreased from the initial 6.4 to 3.2 within the first few minutes.

To check if 4-nitropyrogallol and 5-nitropyrogallol are stable at pH=9, oxidation of 4-nitrocatechol was carried out in basic solution – results are presented in Fig. S8.

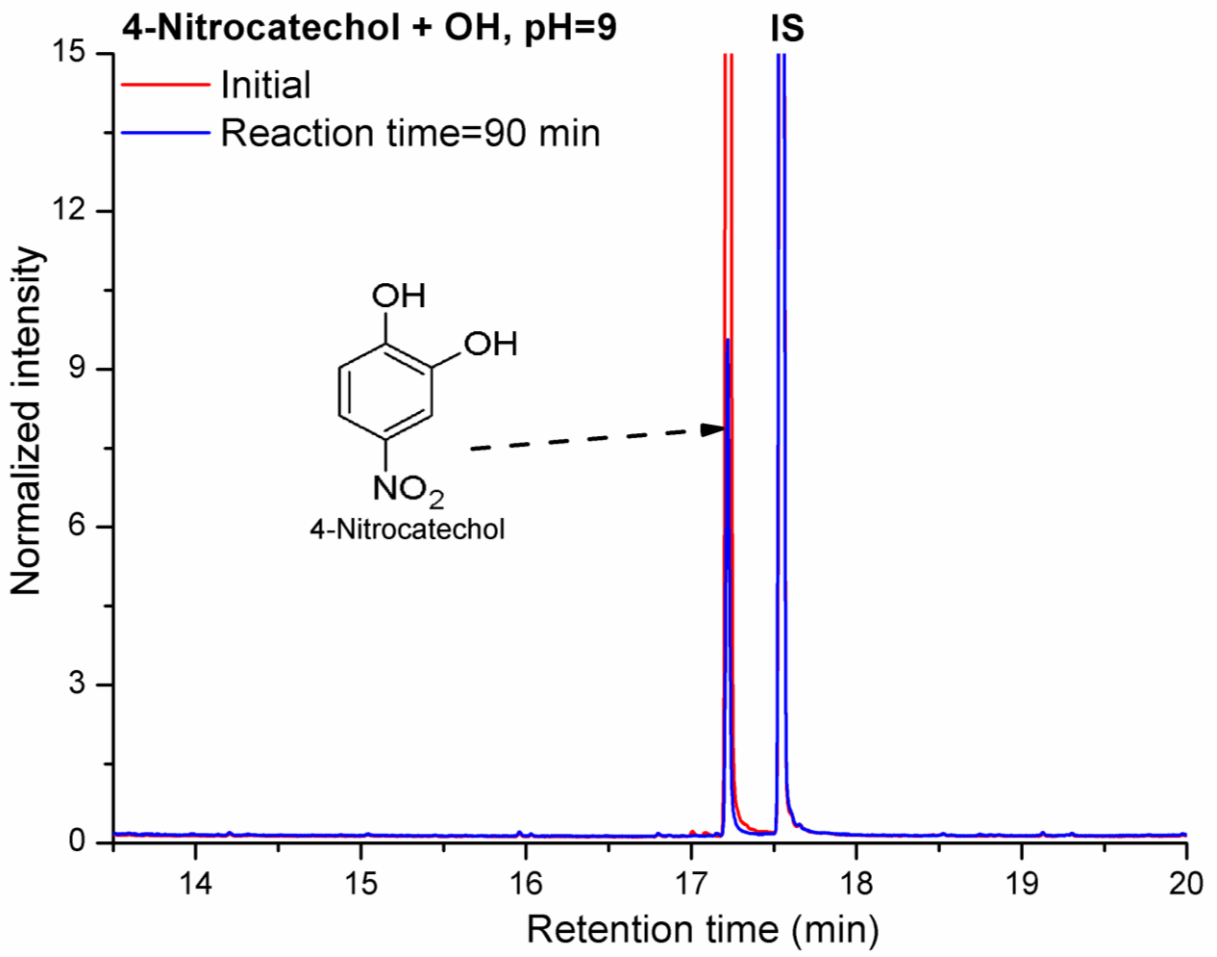

Figure S8: Chromatograms illustrating the formation of phenolic products from OH+4-nitrocatechol oxidation at pH=9.

As presented in Fig. S8, the experimental data acquired confirmed that 4-nitropyrogallol and 5-nitropyrogallol were unstable at pH=9, because chromatographic peaks corresponding to these products were not observed.

S9. Evolution of light absorption of the reaction solution during reaction with OH

UV-Vis spectra, illustrating the evolution of the UV-Vis absorbance of the reaction solution and formation of the light-absorbing products are presented in Fig. S9.

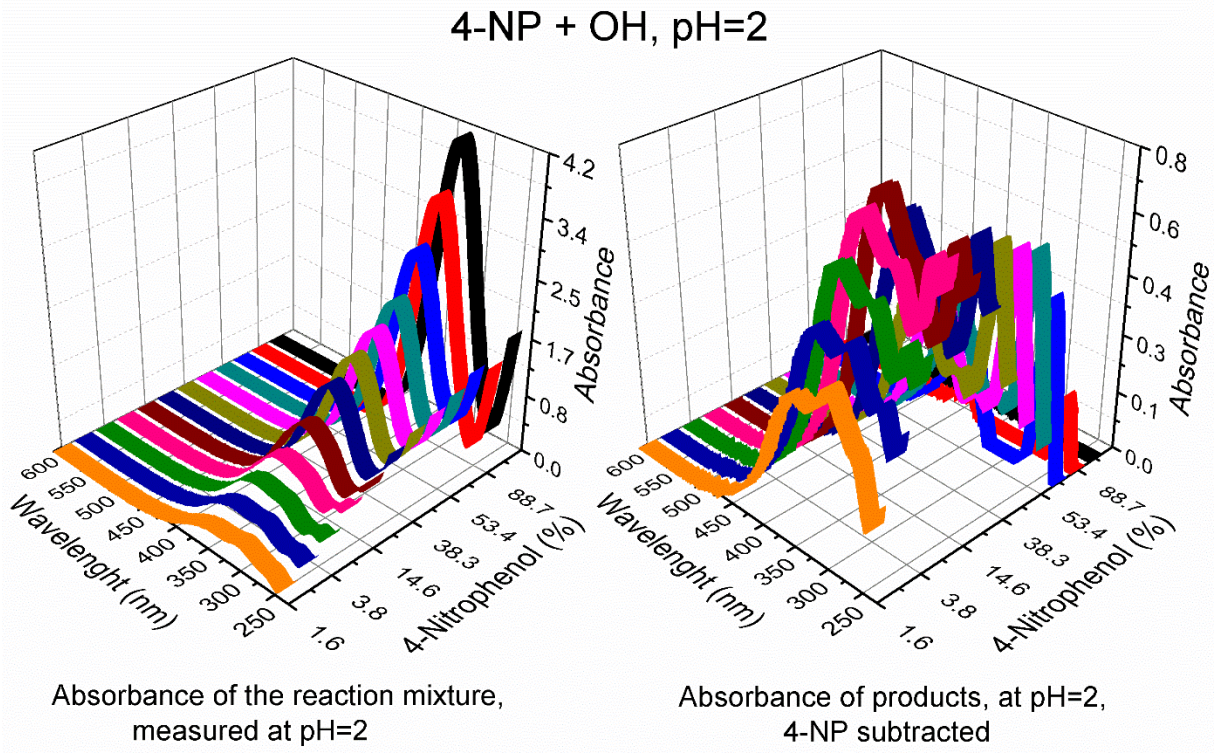

Figure S9: Evolution of the UV-Vis absorbance of the reaction mixture between 230 and 600 nm, the reaction was carried out at pH=2 and the absorbance was measured at pH=2.

As presented in Fig. S9, the absorbance of the reaction mixture shows a steady decrease following the oxidation of 4NP via OH. The absorbance of products was calculated by subtracting the absorbance of 4NP from the measured absorbance of the reaction mixture using eq. SI

$$A_{products}(nm) = A_{r.mix}(nm) - A_{4-NP}(nm) \quad (SI)$$

The pH-dependent absorbance of 4NP was calculated with eq. SII using the [4NP] measured with GC/MS and pH as well as wavelength-dependent molar absorption of 4NP (ε; $mol^{-1} \times L \times cm^{-3}$):

$$A_{4-NP}(nm) = \frac{[4-NP] \times \varepsilon}{Ln(10)} \quad (SII)$$

As presented in Fig. S9, the reaction of OH with 4NP was generating light-absorbing products. For this reason, the bleaching 4NP by OH is prolonged - Fig. S10.

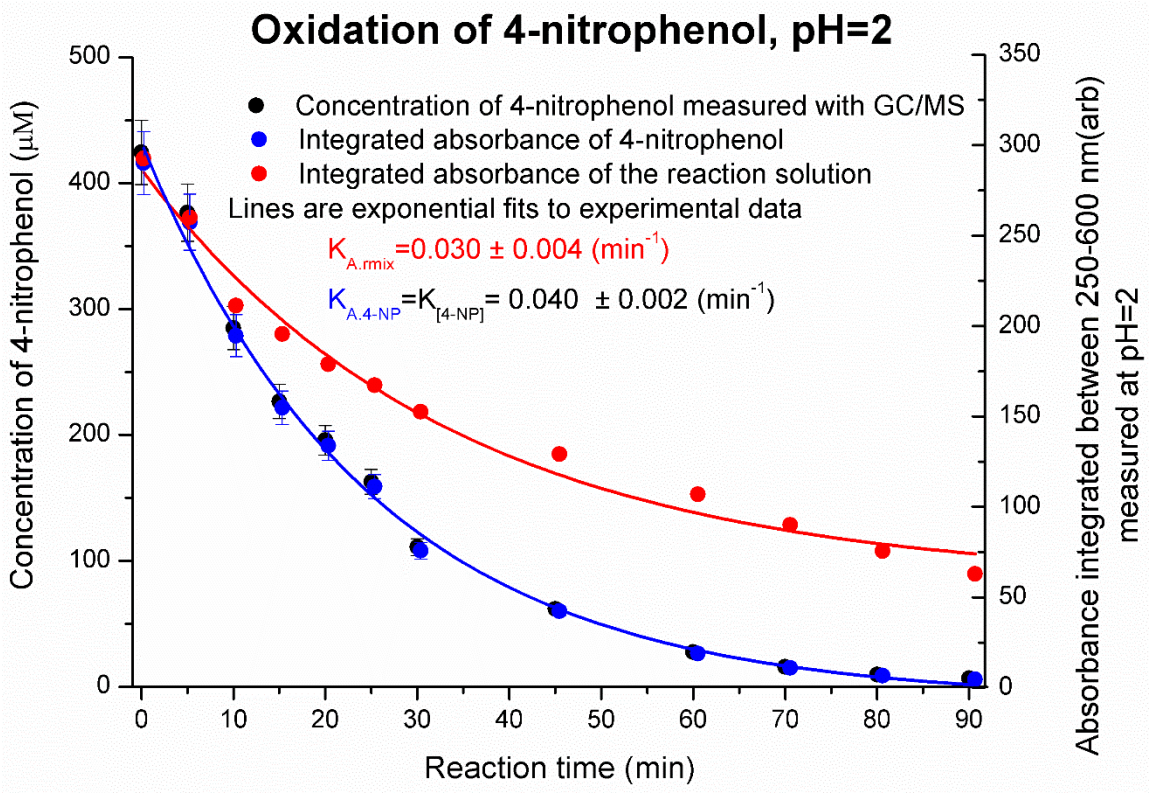

Figure S10: Prolonged bleaching of the chromophores in the 4NP solution due to formation of light-absorbing by-products at pH=2.

As presented in Fig. S10, the disappearance of the integrated absorbance of the reaction solution was slower than the disappearance of the integrated absorbance of 4NP due to the formation of the light-absorbing products. To estimate the atmospheric lifetimes of the chromophores with a significant light absorption between 250 and 600 nm, the empirical $k_{bleaching}$ rate constant was calculated using eq. III. The first order-disappearance rates of integrated absorbance ($K_{A.rmix}$ and $K_{A.4NP}$) were obtained via exponential fit to the experimental data shown in Fig. S10. The empirical $k_{bleaching}$ rate constants were derived using eq. III and experimental data and are listed in Table S4; these rate constants were used to estimate the atmospheric lifetimes of 4NP BrC, as described in more detail in section S12.

To quantitatively evaluate the formation of light-absorbing products under a given reaction conditions, the K_{abs} factor was introduced (eq. II). K_{abs} is used to describe the dependence between the normalized concentration of 4NP and the $(\int_{250nm}^{600nm} A_{10}^{R.mix} d\lambda) / (\int_{250nm}^{600nm} A_{10}^{4NP} d\lambda)$ ratio via eq. II.- Fig. S11.

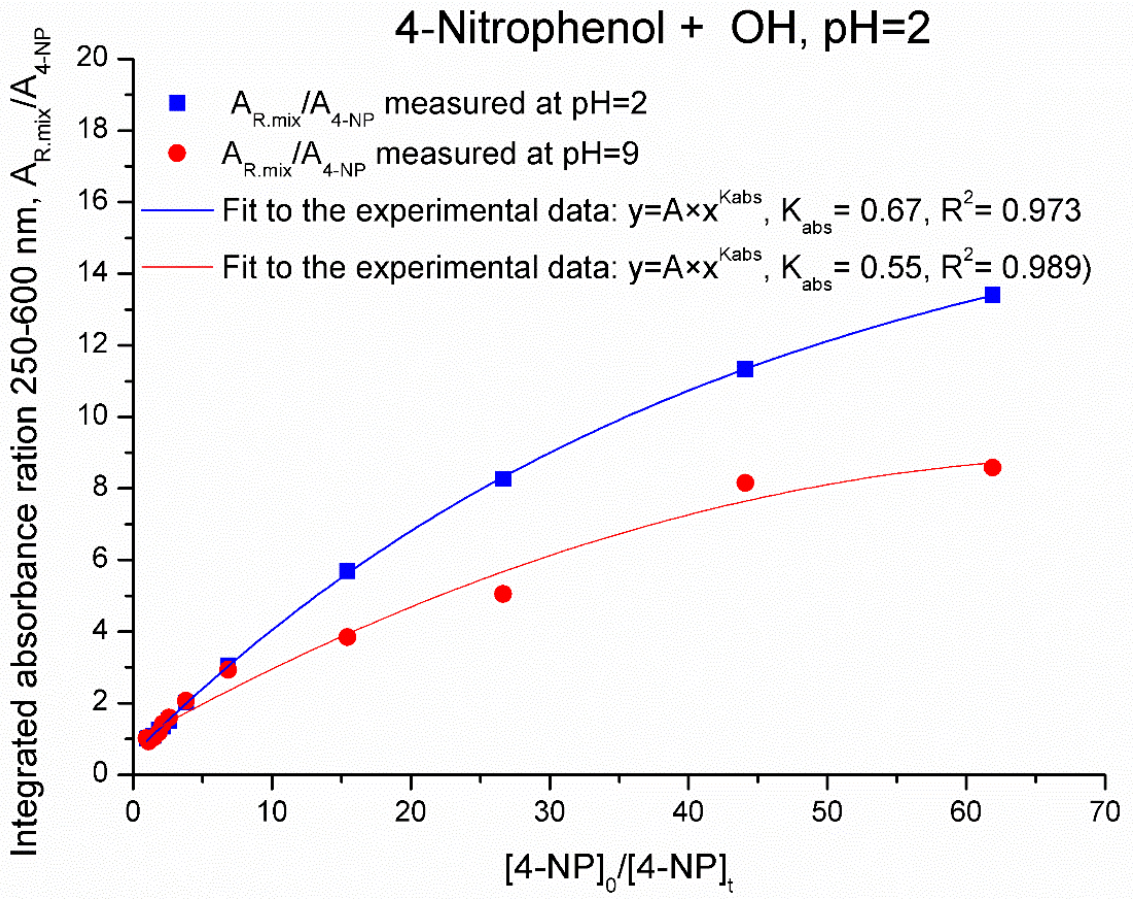

Figure S11: Sample data illustrating the derivation of K_{abs} factors via eq. II.

As presented in Fig. S11, the lower value of K_{abs} corresponds to decreased ability of the reaction (1) to generate the light-absorbing products that essentially prolong the lifetime of BrC chromophores in the solution of 4NP, under given reaction condition (pH). In other words, the absorption of the reaction mixture corresponding to the reaction products increases slower under a given conditions. K_{abs} factors were obtained for the reactions carried out in acidic and basic solutions. Consequently, for the experiments carried out at pH=2 and pH=9, eight K_{abs} factors were obtained because the absorption of the reaction solution was measured between pH=2 and 9 using intervals of 1 pH unit.

The K_{abs} derived were subsequently plotted against the pH at which the absorbance was measured for the reaction carried out under acidic and basic pH - results are presented in Fig. 4 in the main text.

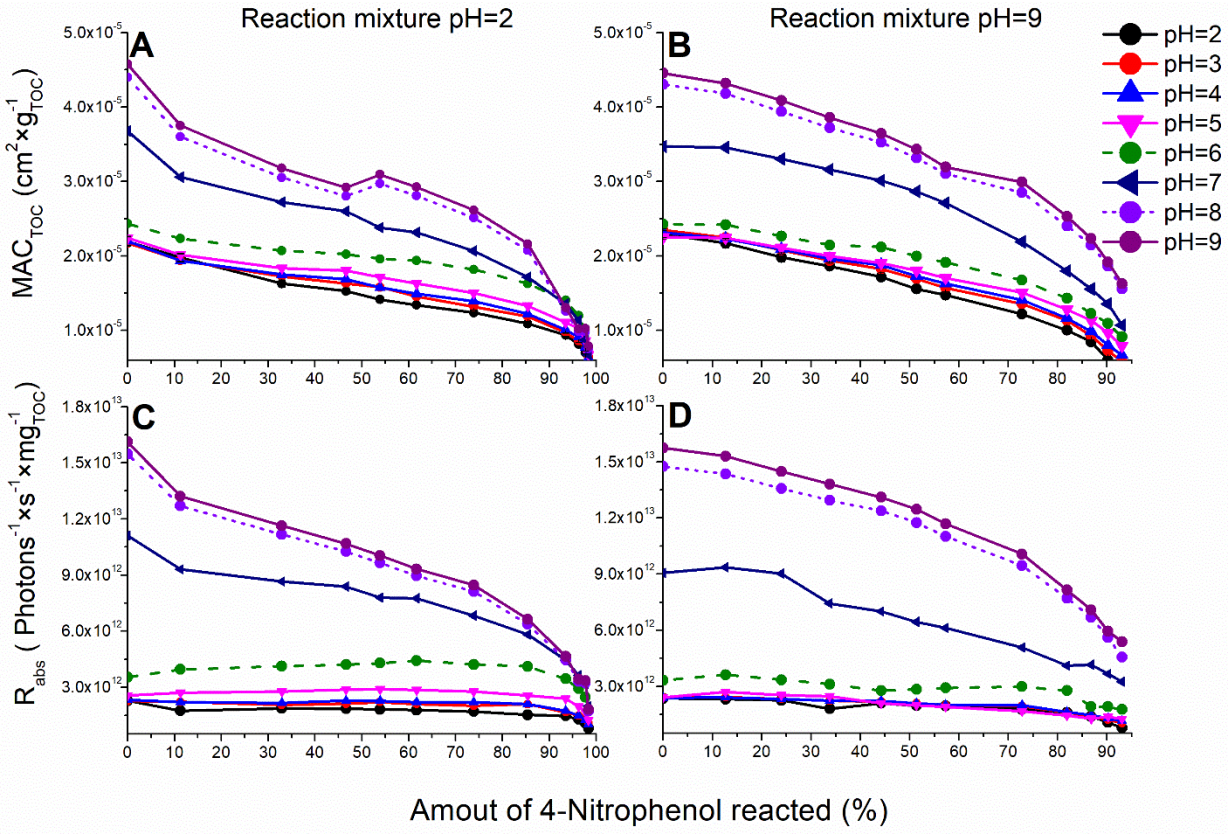

Figure S12: The pH-dependent organic carbon-based mass absorption coefficients (MAC_{TOC}) obtained using the integrated absorbance of the reaction mixture measured for the reaction of 4NP(A) and 4NPT (B) and the corresponding TOC-normalized rates of sunlight absorption (R_{abs}) for of 4NP (C) and 4NPT (D).

Note that the uncertainties (see section 2.7) for the experimental points presented in Fig. S12 and Fig.5 in the main text were derived from UV-Vis and TOC measurements. However, the uncertainties of raw data generated by these instruments were usually very low; 2σ values from three or more measurements were often well below 3%. For this reason, uncertainties bars in both Figs. 4 and S12 are not visible.

S10. Air-water partitioning of 4NP

The partitioning of 4NP between aqueous and gaseous phases as a function of LWC of atmospheric particles (Herrmann et al., 2015) is presented in Fig. S13; it was estimated based on Henry's law constant – the average experimentally measured value is 5×104 ($M \times atm^{-1}$) (Sander, 2015).

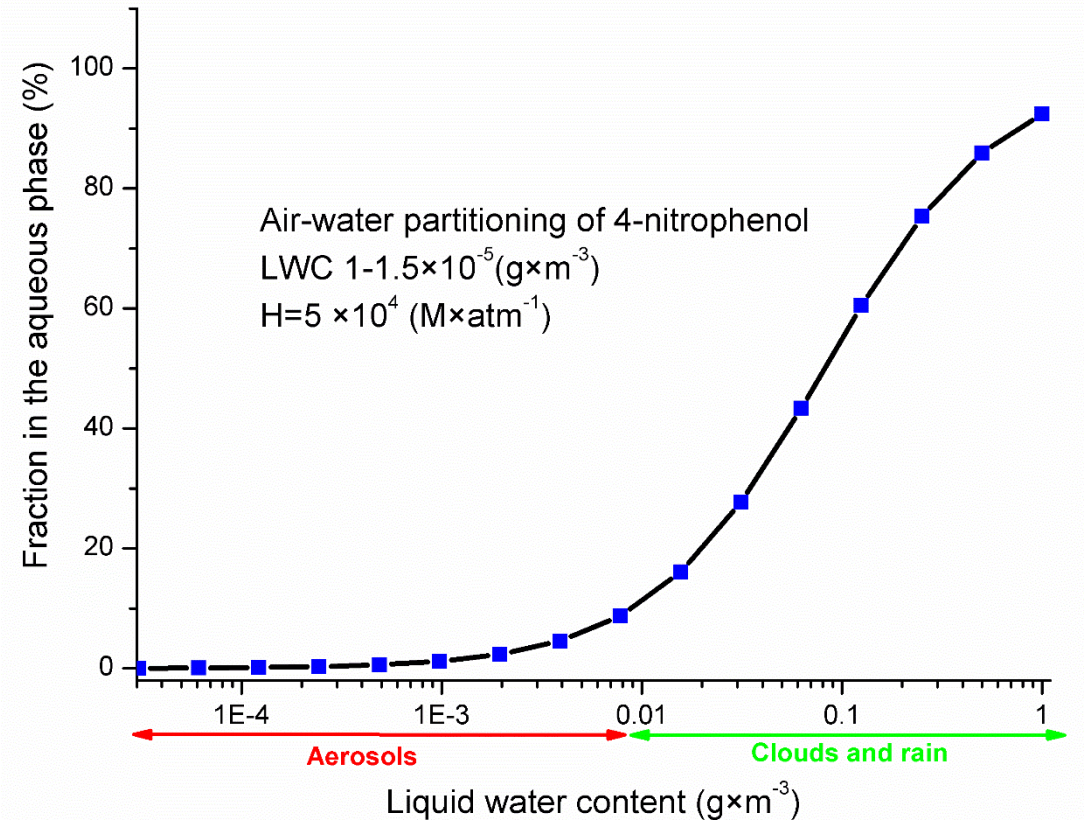

Figure S13: Partitioning of 4NP based on Henry's law equilibrium as a function of liquid water content.

S11 Atmospheric lifetimes and processing of 4NP BrC

Atmospheric lifetimes for bleaching of 4NP due to reaction with OH were calculated with eq. SIII.

$$\tau_{OH}(h) = \left(k_{bleaching} \times [OH]\right)^{-1} \times 3600^{-1} \quad (SIII)$$

In eq. SIII, $k_{bleaching}$ are the empirical rate constant, ($M^{-1}s^{-1}$) for the bleaching of the aqueous solution of 4NP/4NPT by OH (Biswal et al., 2013) calculated with eq. III. [OH] is the aqueous concentration of OH, in cloud water (Herrmann et al., 2010). Atmospheric lifetimes for bleaching of 4NP due to direct photolysis were calculated with eq. SIV.

$$\tau_{photolysis}(h) = \left(\int_{250nm}^{600nm} \phi \times \varepsilon_{\lambda} \times I_{\lambda} \times 1000 \times N_A^{-1}\right)^{-1} \times 3600^{-1} \quad (SIV)$$

In eq. SVI, ϕ is the quantum yield (molecules $\times$photon^{-1}), ε is a wavelength and pH-dependent absorption cross-section measured in this work for 4NP (pH=2) or 4NPT (pH>8) - see appendix 1 and Fig. S5 ($mol^{-1} \times L \times cm^{-1}$), I_{λ} is an actinic flux (photons$\times$ $s^{-1}\times$ $cm^{-2}\times nm^{-1}$) estimated with TUV calculator (Ncar, 2016) for zenith angles 0-50° (Fig. S14) and N_A is Avogadro constant.

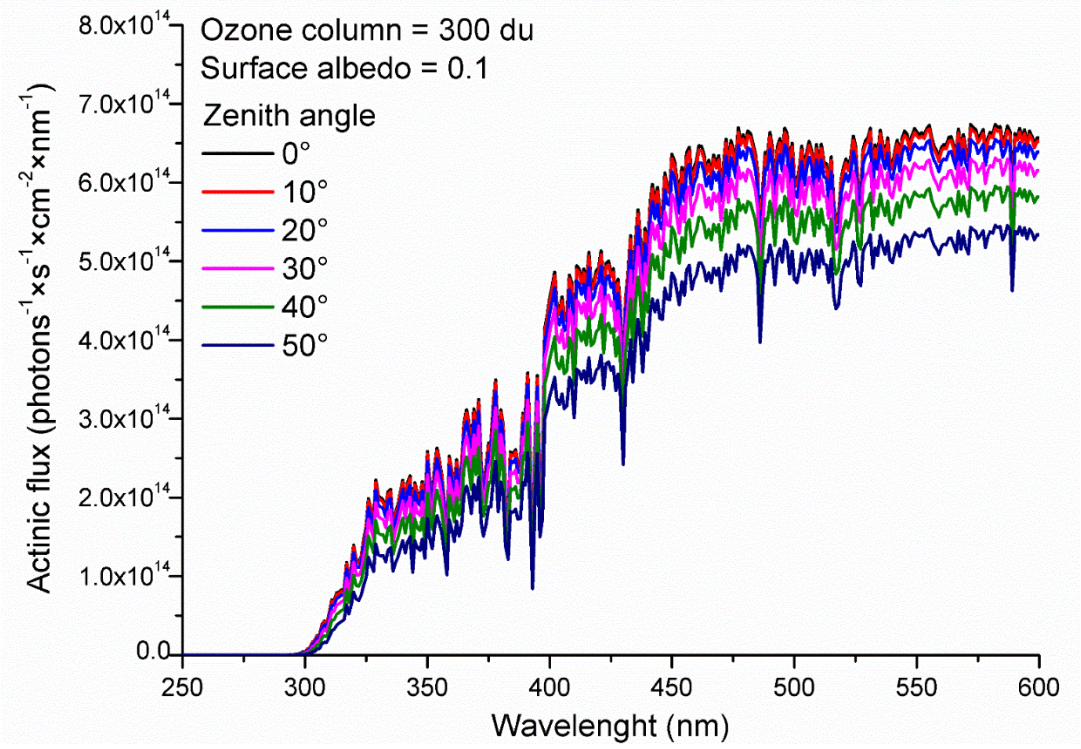

Figure S14: Actinic fluxes estimated with TUV calculator used to derive the R_{abs} values shown in Fig. 5 and photolysis lifetimes shown in Fig. 6. in the main text.

The data used to estimate the atmospheric lifetimes of 4NP-derived atmospheric BrC is listed in Table 1 in the main text.

S12 Mineralization and formation of volatile products

Mineralization of the precursor following reaction (I) was investigated with a TOC analyzer (sections 2.5 and S4.4); the results are presented in Fig.7 in the main text. Note that very similar data from the TOC measurements were obtained when the reaction was carried out at pH=2 and 9. For this reason, only the data for the unbuffered solution is presented in Fig.7. The results of TOC measurements confirmed that after 4NP was completely consumed, 85% of organic carbon remains in the aqueous phase, similar results were also reported previously (Zhang et al., 2003; Liu et al., 2010). This indicates that, following reaction (I), the precursor is primarily converted into ring-opening products. These ring opening products are evidently characterized by the lower UV-Vis absorption as compared with phenols quantified in this work, resulting in a decrease in the absorption of the reaction solution (Fig. 5). These results are in good agreement with the observed decrease in the absorption of the reaction solution.

References

Biswal, J., Paul, J., Naik, D. B., Sarkar, S. K., and Sabharwal, S.: Radiolytic degradation of 4-nitrophenol in aqueous solutions: Pulse and steady state radiolysis study, Radiat. Phys. Chem., 85, 161-166, https://doi.org/10.1016/j.radphyschem.2013.01.003, 2013.

MarvinSketch 20.1 was used for estimating pKa values of 4NC, ChemAxon (https://www.chemaxon.com), last

Hems, R. F. and Abbatt, J. P. D.: Aqueous Phase Photo-oxidation of Brown Carbon Nitrophenols: Reaction Kinetics, Mechanism, and Evolution of Light Absorption, ACS Earth Space Chem., 2, 225-234, 10.1021/acsearthspacechem.7b00123, 2018.

Herrmann, H., Hoffmann, D., Schaefer, T., Bräuer, P., and Tilgner, A.: Tropospheric Aqueous-Phase Free-Radical Chemistry: Radical Sources, Spectra, Reaction Kinetics and Prediction Tools, ChemPhysChem, 11, 3796-3822, https://doi.org/10.1002/cphc.201000533, 2010.

Herrmann, H., Schaefer, T., Tilgner, A., Styler, S. A., Weller, C., Teich, M., and Otto, T.: Tropospheric Aqueous-Phase Chemistry: Kinetics, Mechanisms, and Its Coupling to a Changing Gas Phase, Chem. Rev., 115, 4259-4334, 10.1021/cr500447k, 2015.

Liu, Y., Wang, D., Sun, B., and Zhu, X.: Aqueous 4-nitrophenol decomposition and hydrogen peroxide formation induced by contact glow discharge electrolysis, J. Hazard. Mater., 181, 1010-1015, https://doi.org/10.1016/j.jhazmat.2010.05.115, 2010.

NCAR TUV calculator: https://www.acom.ucar.edu/Models/TUV/Interactive_TUV/, last access: Sep 2021.

Randolph, C., Lahive, C. W., Sami, S., Havenith, R. W. A., Heeres, H. J., and Deuss, P. J.: Biobased Chemicals: 1,2,4-Benzenetriol, Selective Deuteration and Dimerization to Bifunctional Aromatic Compounds, Org Process Res Dev, 22, 1663-1671, 10.1021/acs.oprd.8b00303, 2018.

Sander, R.: Compilation of Henry's law constants (version 4.0) for water as solvent, Atmos. Chem. Phys., 15, 4399-4981, 10.5194/acp-15-4399-2015, 2015.

Tan, Y., Perri, M. J., Seitzinger, S. P., and Turpin, B. J.: Effects of Precursor Concentration and Acidic Sulfate in Aqueous Glyoxal−OH Radical Oxidation and Implications for Secondary Organic Aerosol, Environ. Sci. Technol., 43, 8105-8112, 10.1021/es901742f, 2009.

Vione, D., Maurino, V., Minero, C., Duncianu, M., Olariu, R.-I., Arsene, C., Sarakha, M., and Mailhot, G.: Assessing the transformation kinetics of 2- and 4-nitrophenol in the atmospheric aqueous phase. Implications for the distribution of both nitroisomers in the atmosphere, Atmos. Environ., 43, 2321-2327, https://doi.org/10.1016/j.atmosenv.2009.01.025, 2009.

Witkowski, B., Al-sharafi, M., and Gierczak, T.: Kinetics and products of the aqueous-phase oxidation of β-caryophyllonic acid by hydroxyl radicals, Atmos. Environ., 213, 231-238, https://doi.org/10.1016/j.atmosenv.2019.06.016, 2019.

Zhang, W., Xiao, X., An, T., Song, Z., Fu, J., Sheng, G., and Cui, M.: Kinetics, degradation pathway and reaction mechanism of advanced oxidation of 4-nitrophenol in water by a UV/H_2O_2 process, J. Chem. Technol. Biotechnol, 78, 788-794, https://doi.org/10.1002/jctb.864, 2003.

Zhao, R., Lee, A. K. Y., Huang, L., Li, X., Yang, F., and Abbatt, J. P. D.: Photochemical processing of aqueous atmospheric brown carbon, Atmos. Chem. Phys., 15, 6087-6100, 10.5194/acp-15-6087-2015, 2015.